Electric Power Systems Research 234 (2024) 110837

Contents lists available at ScienceDirect

Electric Power Systems Research

journal homepage: www.elsevier.com/locate/epsr

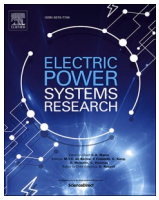

Fault analysis for DC Bus-integrated energy storage system, electric vehicle supply equipment, and photo voltaic systems

Kirn Zafar [a], Mohamed K. Kamaludeen [a,b], Yusef Esa [a,b], Ahmed Ali A. Mohamed [a,*], Simon Odie [b]

[a] Smart Grid Interdependencies Laboratory, Department of Electrical Engineering, Grove School of Engineering, City University of New York City College, New York, NY 10031, USA
[b] Consolidated Edison of New York, New York, NY 10003, USA

ARTICLE INFO

Keywords:
Direct current (DC) Bus
DC microgrids
Distributed Energy Resources (DERs)
Grid interconnection
DC Circuit Breakers (DCCBs)

ABSTRACT

Reliable access to cost-effective electricity is the backbone of the U.S. economy, and energy storage is an integral element of the power system with high penetration of Distributed energy resources (DERs). Investment in energy storage is essential for keeping pace with the increasing demands for electricity arising from continued growth in U.S. productivity, continued expansion of national cultural imperatives (e.g., emergence of the distributed grid and electric vehicles), and the projected increase in DERs. This research is on the forefront of this transition with fault analysis execute for a real system to be implemented in New York City at a Utility substation. The project seeks to pair a grid-connected battery energy storage system (BESS), solar photovoltaic (PV) system, and an electric vehicle charging system (EVCS) on a common DC bus. A transient model has been developed and different fault scenarios (i.e., high-impedance and low-impedance faults) have been simulated, at various points of the system for several durations. The objective of this study is to determine the requirements for electrical protection equipment, i.e., DC Circuit Breakers (DCCBs) in terms of capacity and fault clearing time that can ensure stable operation of the DC bus system while meeting the utility and IEEE requirements for system stability. The results showed that fast-response DCCBs is a key element for the system. Solid-State DC breakers with ultra-high speed must be deployed for prompt detection/isolation of faults. Actual ratings of converters and allied equipment need to be considered before the finalization of ratings and specification of protection equipment.

1. Introduction

DC microgrids consist of distributed energy resources (DERs) and loads, e.g., fuel cells, Electric Vehicles (EVs), solar Photovoltaics (PVs), wind power generation, and battery energy storage systems, controlled via a control and communication system [1]. DC microgrids are promising solutions to achieve reliability and resiliency in future power grids. They enhance the utilization efficiency of DERs, offer better power quality, result in less electromagnetic compatibility issues, and mitigate cyber security concerns. Further, challenges related to eddy current losses, skin effect, reactive power compensation, and AC-DC conversion are eliminated with the use of DC systems [2-4]. The motivation behind the planning and development of this DC bus pilot project by the utility is the fact that the interconnection of DC-based DERs has the potential to become more efficient. In this regard, this study is based on the fault analysis of a pilot project to be deployed by Consolidated Edison Inc. in New York City.

In this project, a BESS based on Lithium Iron Phosphate will be installed at a substation. The load area of Larchmont, Southern New Rochelle and some parts of Mamaroneck are fed by that substation. The location of the substation resides along major interstate rail line (Metro-North) and I-95 interstate highway known for heavy vehicular traffic. This proximity coupled with available space at an adjacent parking lot next to the substation, makes it an ideal location to install EV charging station to support the corridor traffic. In addition, with the Utility-Owned BESS situated at the substation, grid operators will now have the flexibility to support resilience operations (via the inherent microgrid) and facilitate DERs deployment in the load area. In this project, 10-DC fast charging station for EVs will be covered by a solar PV canopy that is owned and operated by a third party and interconnected to the

* Corresponding author.
E-mail address: amohamed@ccny.cuny.edu (A.A.A. Mohamed).

https://doi.org/10.1016/j.epsr.2024.110837
Received 6 March 2024; Received in revised form 27 May 2024; Accepted 18 June 2024
Available online 24 June 2024

Table I
Summary of Literature Review and Research gap.

Ref	Objectives	System under Consideration	Validation/Fault analysis of Real Time System
[21]	Designing a scheme for estimating the fault distance based on the peak features by using only local measured values. Utilization of local measurements to estimate fault distance.	A 3 km line segment of a dc microgrid	No
[22]	A scheme is proposed to identify faults based on voltage and current of DC link capacitor.	Ring bus DC microgrid	No
[23]	A sliding discrete Fourier Transform based scheme is proposed to identify and limit the fault.	5-bus DC microgrid system	No
[24]	Fast Fourier Transform is used to compute real and imaginary parts of power. Protection scheme is proposed for fault diagnostic and isolation.	IEEE 9 bus system	No
[25]	Wavelet Transform based protection scheme is proposed.	Low Voltage DC microgrid	No

BESS at the substation via a common DC bus. Several analyses have been carried out by the authors to determine the feasibility, cost-effectiveness, and detailed design and modeling of the DC bus. A transient model has been developed and different fault scenarios (i.e., high-impedance and low-impedance faults) have been simulated, at various points of the system for several durations. The rest of the paper is organized as follows: In Section II, a literature review regarding the protection and fault analysis of DC microgrids has been presented. Section III elaborates on the system configuration under study. Section IV pertains to the simulation of fault analysis and discussion of results. Finally, conclusions and recommendations for the system under study are discussed in Section V.

2. Literature review

Various studies have been carried out to investigate the feasibility of DC system utilization for the distribution of power [5-6,8]. However, most of the DC systems deployed to date find applications on shipboards, data centers, small-scale EV parking, and part of laboratory testbed demonstrations [9,10]. Even though the advantages of DC systems have been established over AC counterparts, widespread deployment of DC systems is still under development. There are several technical challenges and obstacles involved in the implementation of DC systems. Specifically, as it relates to protection, grounding, and stability each of which is discussed extensively in this literature section.

2.1. Protection-Related challenges of DC microgrids

DC Microgrids (DCMGs) have been the focus of many researchers over the years. However, more efforts are needed, especially regarding stability, protection, grounding, control, and standards, for realization of DCMGs. Some of the key issues surround the optimizing operation and control of the DERs and storage systems by controllers. Moreover, voltage regulation, sharing of load currents, and parallel operation of multiple DC-DC converters are main factors, which may pose challenges for traditional controllers. The issues and challenges associated with the protection of DCMG have also been elaborated in [11–13] and [16].

Another factor to consider are the characteristics of DC bus short circuit current and how system parameters vary during faults in DC systems. The rate of rise in DC fault currents is extraordinarily high as compared to the fault currents in AC systems. Various topologies, configurations, and operation modes of DCMGs demand a carefully

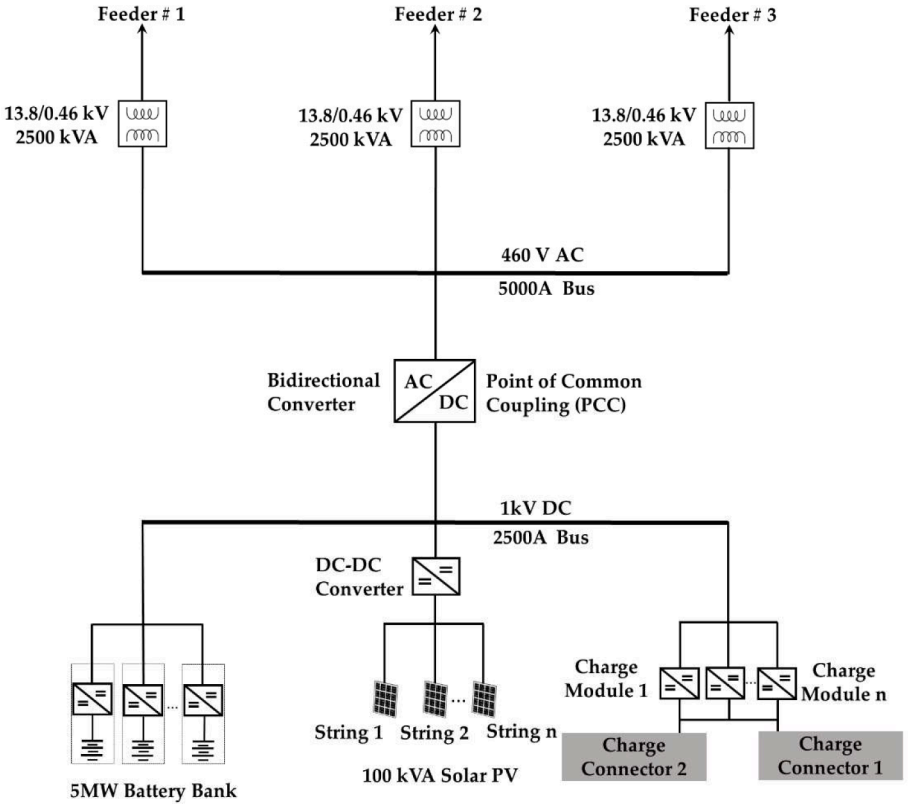

Fig. 1. Single line diagram for the system under study.

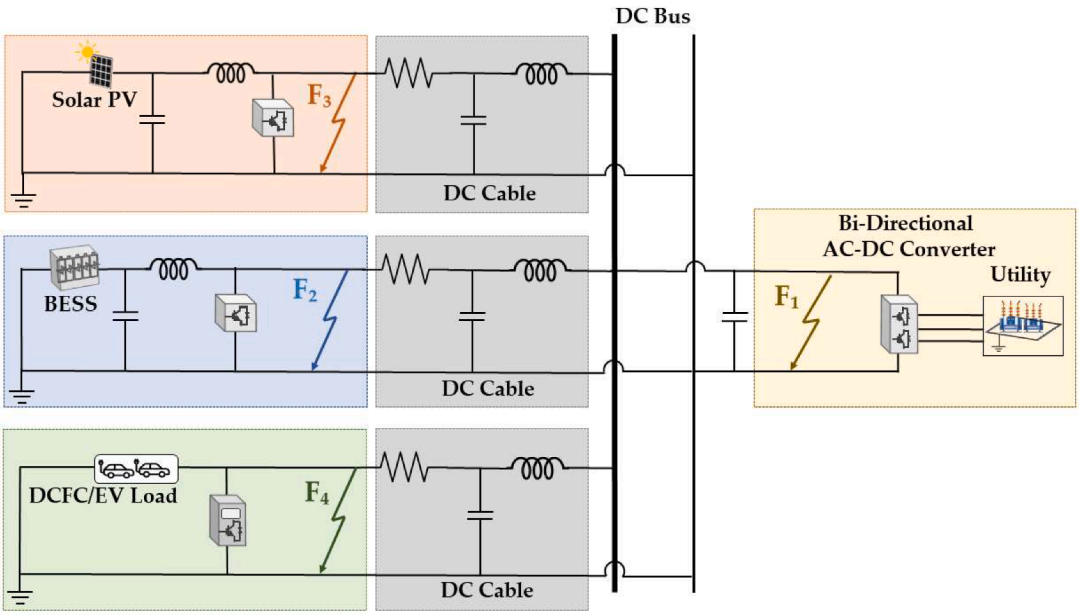

Fig. 2. Schematic Diagram showing simulated PP fault locations.

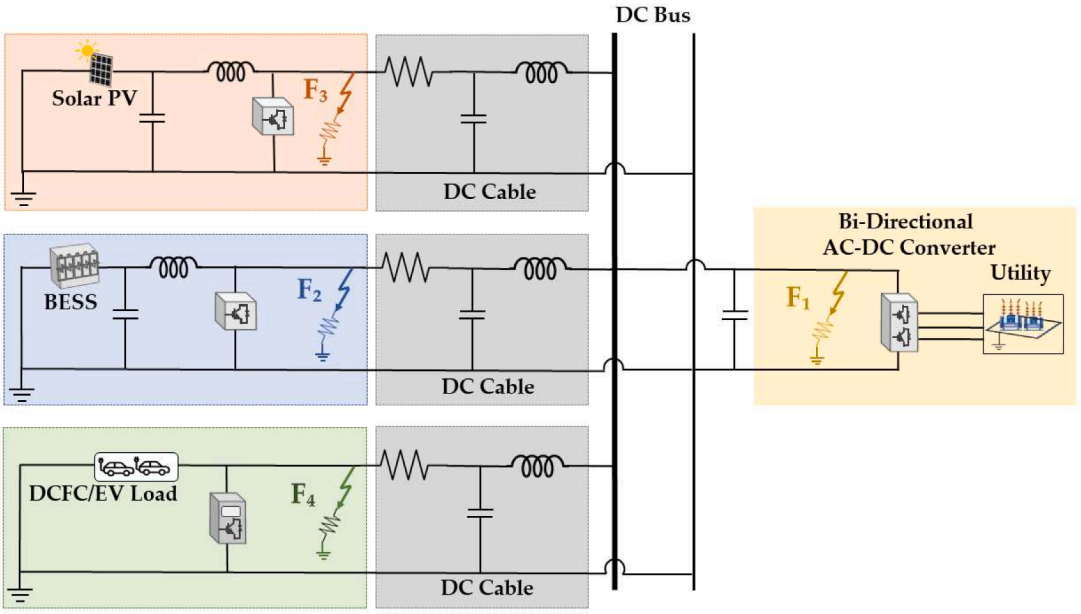

Fig. 3. Schematic Diagram showing simulated PG fault locations.

designed and reliable protection system with consideration for the uniqueness of the systems. Protection of DCMGs is classified into three stages i.e., detection, isolation, and reconfiguration of faults. Fault management can be carried out well if the system behavior during faults is understood. Also, system stability and fast restoration can be achieved even when the characteristics of fault differ from traditional AC faults e.g., absence of zero crossing, ultra-high rate of rise of fault currents etc.

2.2. Ground- Related Challenges of DC microgrids

To cope with the challenges pertaining to fault management of DCMGs, techniques such as appropriate grounding, approaches for intelligent fault detection and appropriate DCCBs play important roles. As highlighted in the DC microgrid model by Nahas et al., [17], the system behavior during a fault can vary widely based on its grounding scheme. Because of this, special attention should be given to DC system ground for grid integration. When a fault is applied on the DC terminals, corresponding response of each DER must be observed for determination of protection techniques. The time constant and magnitude of fault current is different for different configuration and sources. Individual fault response of each component is obtained and compared with the results of the scenario where all the sources are connected to DCMG system. It has been concluded, with respect to various fault types and fault locations, that the contribution to the fault currents from the batteries is the highest among all other components. Relief is provided by the batteries in case of voltage collapse which can result into the lower contributions of the fault currents from DER systems. Fault detection becomes difficult in case of pole to ground faults because the contribution of faults from PV and wind systems becomes lower. The contribution of steady state fault current from each unit will be affected

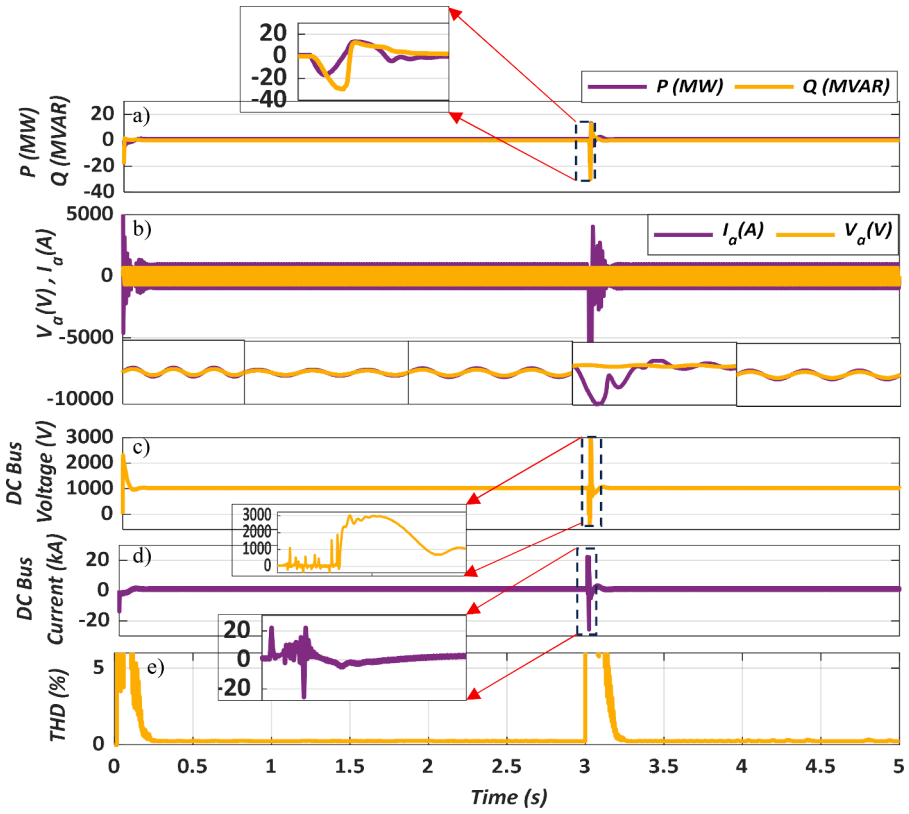

Fig.4. Results for Case 1a. a) P, Q b) V_{ac}, I_{ac}, c) DC bus voltage d) DC bus current e)%THD.

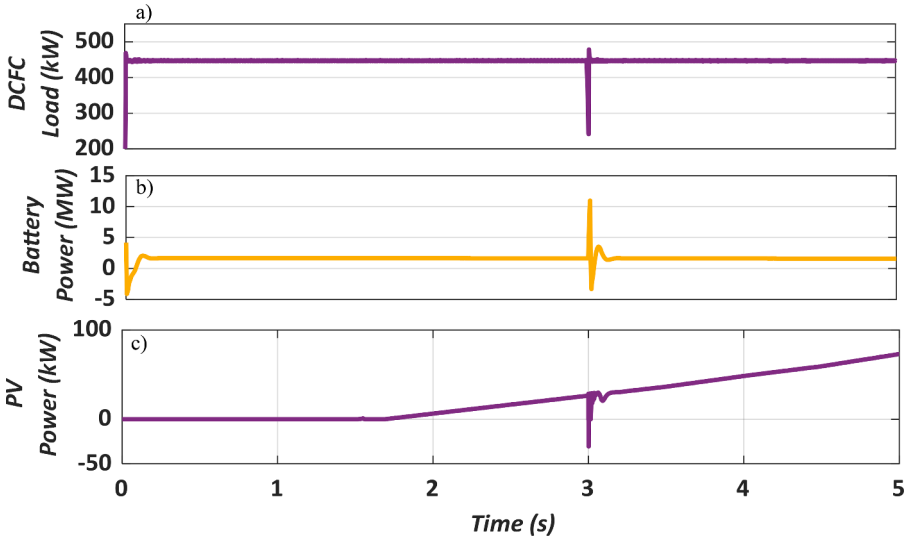

Fig. 5. Results for Case 1a. a) DCFC load b) *P* battery c) *P* from solar PV system.

significantly because of change in fault resistance, especially in case of fault on the transmission line of any unit. Further, power electronics interface, control schemes also impact the characteristics of fault currents which should be factored into designing protection schemes for the DC microgrids.

One of the major challenges related to DC current is the lack of zero crossing, which makes it challenging to extinguish the arc during fault current interruption. The rate of rise of DC fault current is fast and steep and requires fast fault interruption devices such as solid-state circuit breakers and hybrid circuit breakers. Depending upon the design and architecture of DCMG, it be connected to the grid via bidirectional inverters at various terminals. However, this configuration may pose a challenge when designing protection schemes to handle fault currents through multiple ports in multi directions. As such, flexibility must be baked in the protection schemes for systems with such configurations. Additionally, different relay settings are required for different modes of operations. Because fault levels and directions do not remain same during islanded, and grid connected modes of the DCMGs [16]. The control of DERs, supply-demand balance, and control and management of the state of charge of energy storage systems may also cause protection-related issues [14]. Further, it is important to design a discriminating protection scheme that can distinguish normal operation

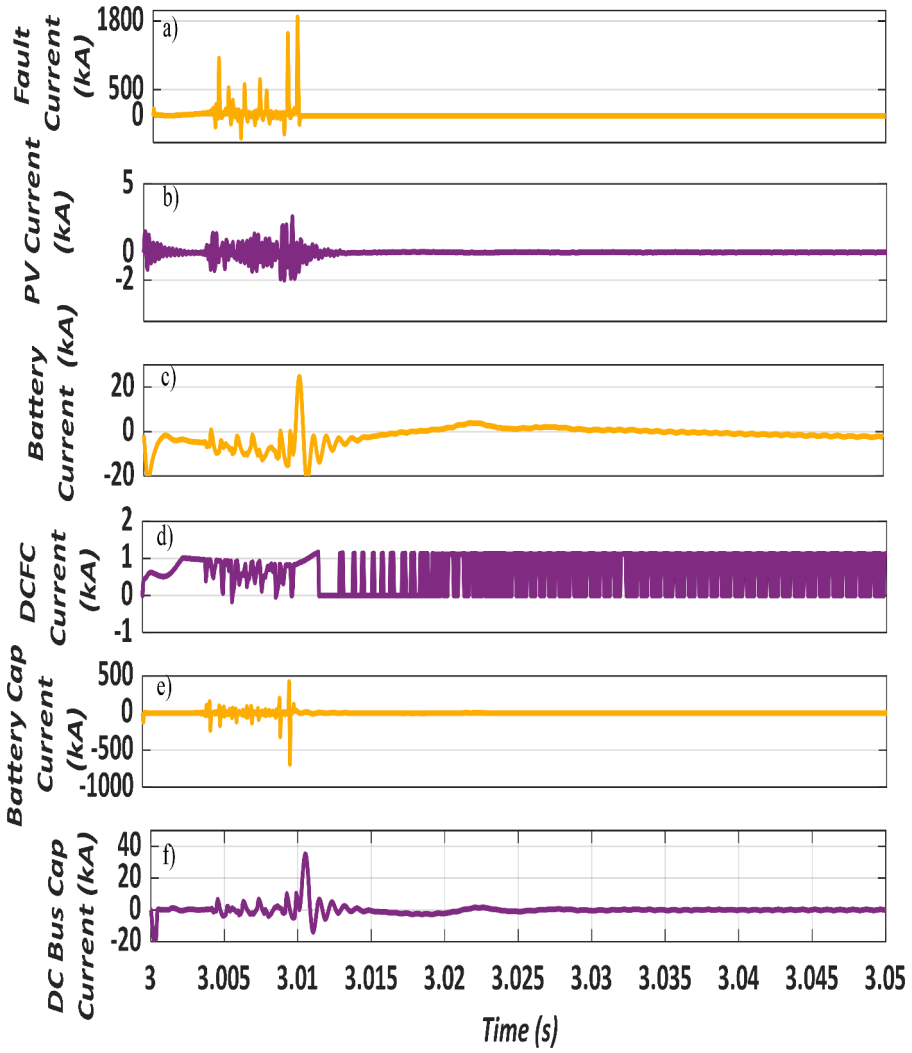

Fig. 6. Results for Case 1*a*. a) Fault current b) Current through PV system c) Current through battery system d) Currents through DCFC e) current through capacitor at battery terminals f) current through capacitor at DC link.

events and events of fault for optimal operations of the DCMGs. The control schemes applied modelling techniques of grounding, DC bus and MG components as well as the interface of power electronic devices affect the characteristics of fault currents in DCMGs. Different features of fault current at various locations of DCMGs have been simulated and analyzed [18]. Besides zero-crossing, there is lack of phasor information and frequency in DC systems, which makes the requirements of DC protection different from AC systems.

In case of a fault on the AC side, the situation can become worse because there is the possibility of flow of AC fault current to the DC side due to the presence of antiparallel diodes in converters. If a solar PV system exists in DCMG, the change in maximum power point (MPP) can result in the instability of the system. Therefore, the selection of proper schemes for ground faults on the solar PV side are crucial. During the occurrence of a fault, the voltage drops, and more current is drawn by constant power loads. This phenomenon is known as “incremental negative resistance” which may result in current or voltage oscillations. The fault current must be reduced, which is also a challenge [15].

The selection of protective equipment for a DC system primarily depends on configuration, system components, and size. Traditional DCCBs have disadvantages of arcing and high fault clearing time. Therefore, hybrid circuit breakers or solid-state circuit breakers must be deployed, which have minimum fault clearing time and less/no arcing. To design the protection system based on these DCCBs, the cost and economic feasibility must be considered [1]. According to the authors of [17], the reliability and security of DCMGs can be ensured only if all the components comprising the MG are protected. Different protection schemes for PV system, wind farms and battery system protection are discussed and compared in [17].

A dynamic and accurate model of DCMG is presented in [18]. The dynamic model comprises of load model, storage, converters, wind turbine and solar PV. The proposed dynamic model can accurately model the system under fault conditions. The accuracy of the analysis is improved particularly during faults.

2.3. *Stability-related challenges of DC microgrids*

The operations of the protective devices, such as relays, can be affected by the transient response of the hybrid microgrid after the fault [19]. This can also impact the voltage stability in the islanded hybrid microgrid. Hence, the analysis of the transients arising from temporary fault is important to make sure the resiliency and stability of the system. Generally, the factors i.e., control parameters of converters and DERs, operating conditions and type of DERs and operating modes of the microgrids. The analysis of the transients produced by faults is not a problem to be solved through mathematics due to the complex interactions between converters, loads and DERs. Therefore, techniques based on simulation are required for analysis. Important applications of

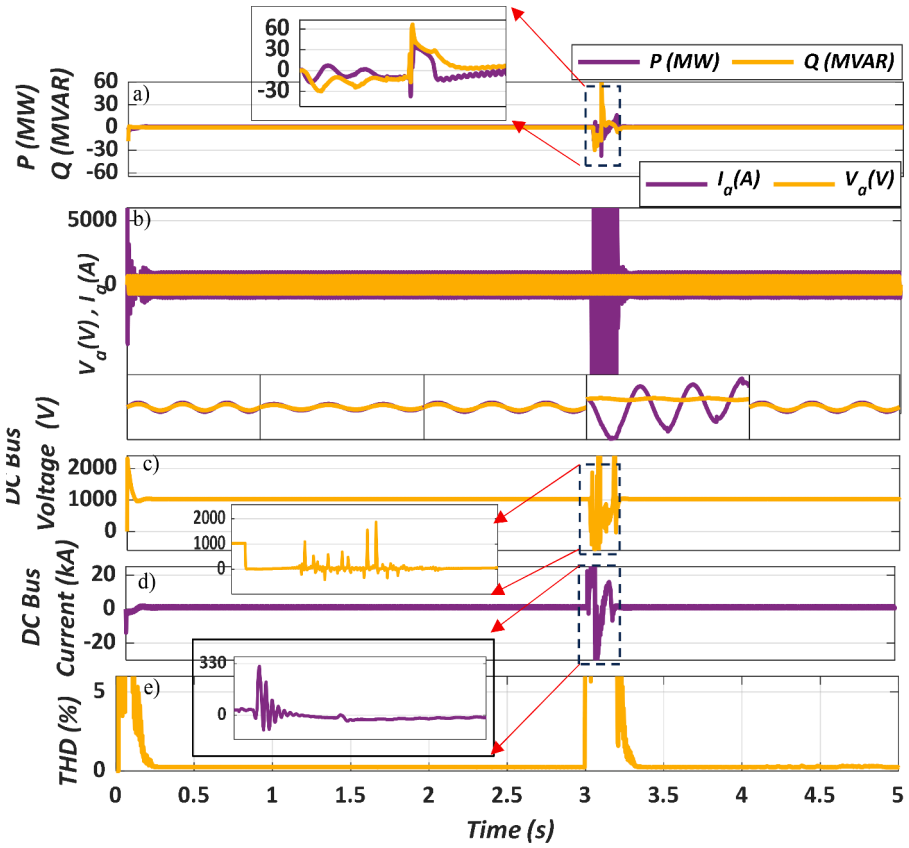

Fig.7. Results for Case 1b a) P, Q b) V_{ac}, I_{ac}, c) DC bus voltage d) DC bus current e) THD vs. Time(s).

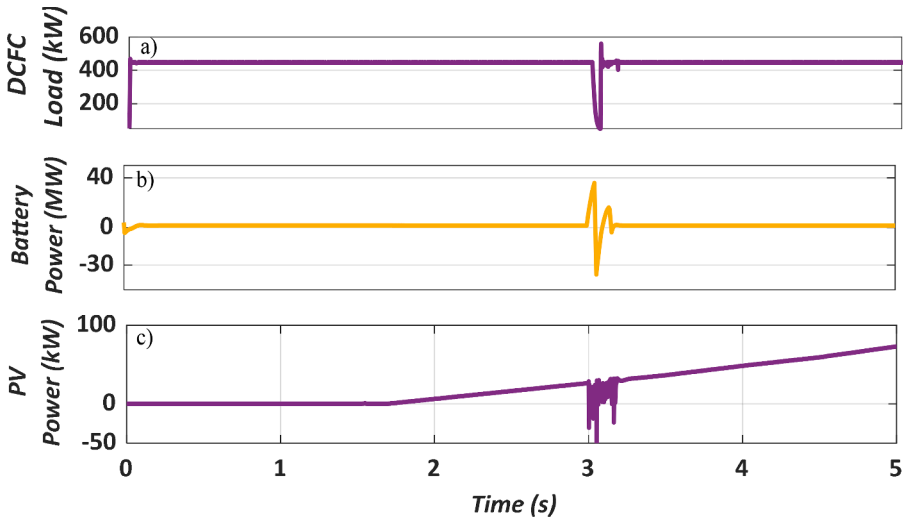

Fig. 8. Results for Case 1*b*. a) DCFC load b) *P* battery c) *P* from solar PV system.

simulation-based methods include Critical Clearing Time (CCT) estimation, fault location-based assessment of sensitivity and resistance. If fault current duration is greater than CCT value, it becomes impossible to recover the voltage of microgrid [20].

DC-AC or DC-DC power converters are coupled with capacitive filters which pose another threat to the system protection. During a fault, the discharge of capacitors can cause a spike in current which may have values up to 10kA to 50kA depending on the installed capacity of converters, location of the fault, and design of filters [1]. As a result of high discharge currents, both up and/or downstream breakers can trip causing an increased level of load interruption. Further, circuit breakers may be damaged due to such a high magnitude of current. The situation could become worst if capacitors connected to the load side also discharge their currents to the fault. Although the discharge current is extremely high, it is only for a small duration, which is not sufficient for CB contacts to completely open. If the inductance is dominant in the system, there is the possibility of contacts being welded closed. Weld-closed and failure to open are major operational issues. In this case, the coordination of tripping and timing in protection schemes is extremely difficult to achieve. However, the situation can be improved with the installation of low-voltage circuit breakers which can ride through high capacitive discharge currents but tends to be more costly

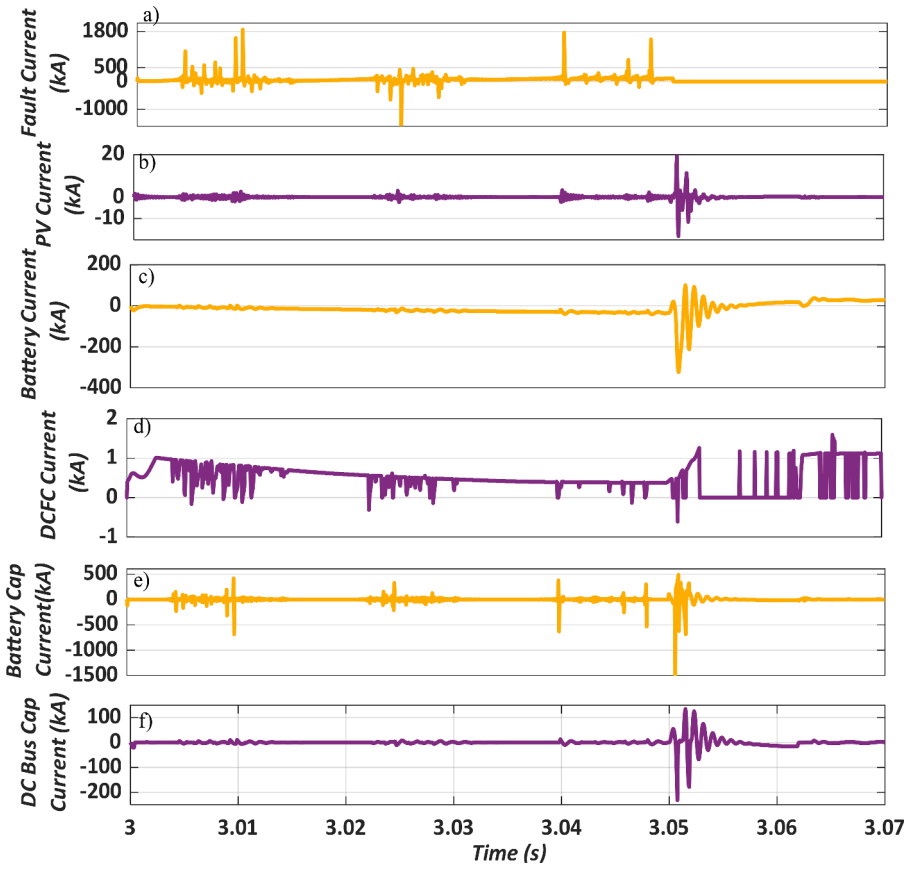

Fig. 9. Results for Case 1*b*. a) Fault current b) Current through PV system c) Current through battery system d) Currents through DCFC e) current through capacitor at battery terminals f) current through capacitor at DC link.

[1].

Communication systems are used for the exchange of control signals or information among controllers depending upon the type of control, i.e., Hierarchical, Distributed or Centralized. The same can also be utilized for exchange of current and voltage measurement for fault isolation. However, the signals pertaining to protection must be communicated faster as compared to the speed of control signals exchange. Hence, to improve the efficiency of DC systems and their protection system, there is a need to discuss their enabling communication network.

2.4. Contributions

Table I shows the research objectives achieved by the researchers and the research gap which still needs to be addressed. The review revealed that several analyses have been performed on protection of DC bus systems and with various recommendations. However, the fault analysis of a real DC bus system for designing the protection schemes has not been presented in the literature to the best of authors' knowledge. In this study the above-mentioned research gap has been abridged. The key contributions are listed as below.

1. Transient modeling of all the elements of DC bus system has been performed. The parameters of the interconnecting cables and grid have been calculated using the data/information obtained from the Utility.
2. The characteristics of fault currents have been analyzed for the DC bus system to be installed at Con Edison's substation.
3. The results of the analysis are helpful in determining not only the capacity (amperes) of the DC circuit breakers (to be installed in the actual system) but also for assessing the maximum fault clearance time. These two factors are reported as the most crucial in the literature review for the implementation of protection schemes in DC bus systems.

3. System design

This section summarizes the proposed design for the DC bus system. A 5MW/20 MWh battery system is owned by the utility; whereas 1MW (10 Electric Vehicle Supply Equipment (EVSE)) and 100 kW solar PV systems are owned by a third party that is connected to the utility-owned battery system via a common DC bus as depicted in Fig. 1. The DC bus voltage is 1000 V, which is linked with an AC bus of 460 V via a bidirectional converter. The voltage of the AC bus is stepped up to 13.8 kV. Further, three distribution feeders are connected through three 2.5 MVA submersible transformers using disconnect switches and breakers. Communication between third-party DERs and New York Independent System Operator (NYISO) will be managed by a local microgrid controller. The utility DC bus voltage will be regulated either by the battery system or the bi-directional converter. Voltage (V), real power (P), and reactive power(Q) set points will be exchanged with SCADA systems.

4. Transient simulation results

A transient simulation model has been developed for the system in MATLAB/Simulink. The Simulink models of various components i.e., DC-DC converter and bi-directional converter have been validated in [4]. The system was simulated for several cases which are explained in this section. There are two types of faults that generally occur in DC microgrids i.e., Pole to Pole (PP) and Pole to Ground (PG). PP faults are also called Low Impedance Faults (LIF) since a path for current is

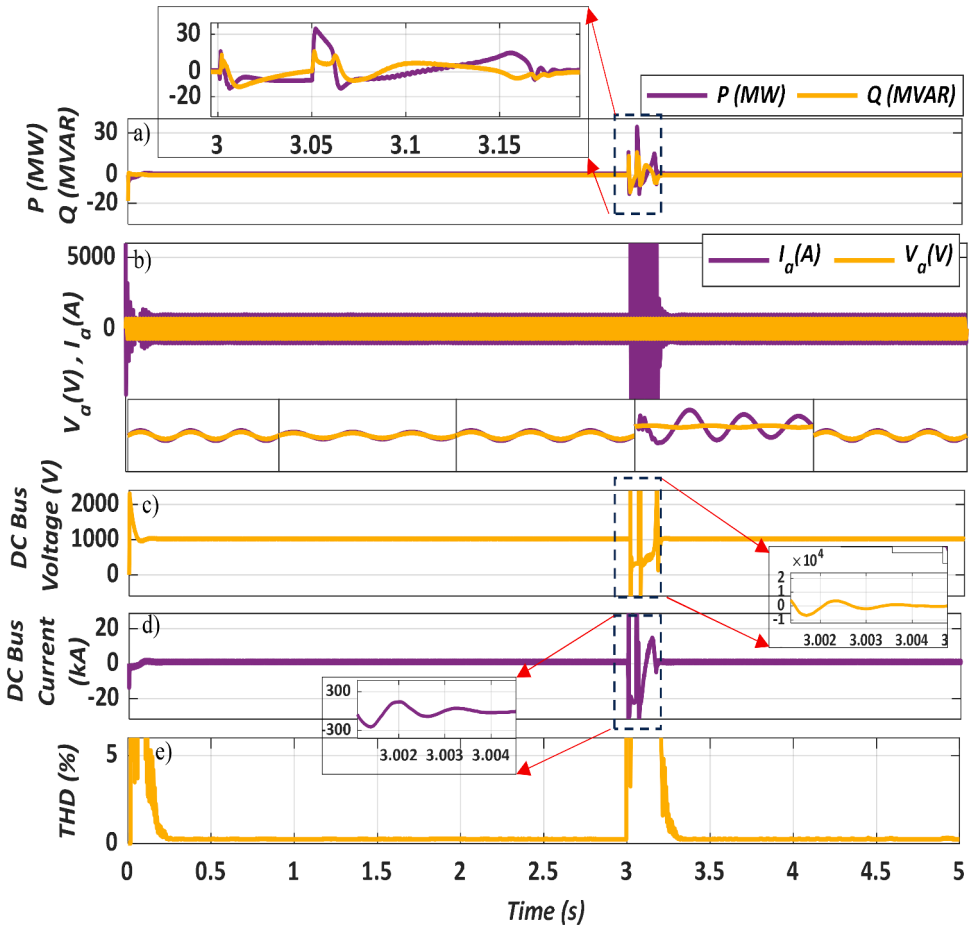

Fig. 10. Results for Case 1c a) P, Q b) V_{ac}, I_{ac}, c) DC bus voltage d) DC bus current e) THD.

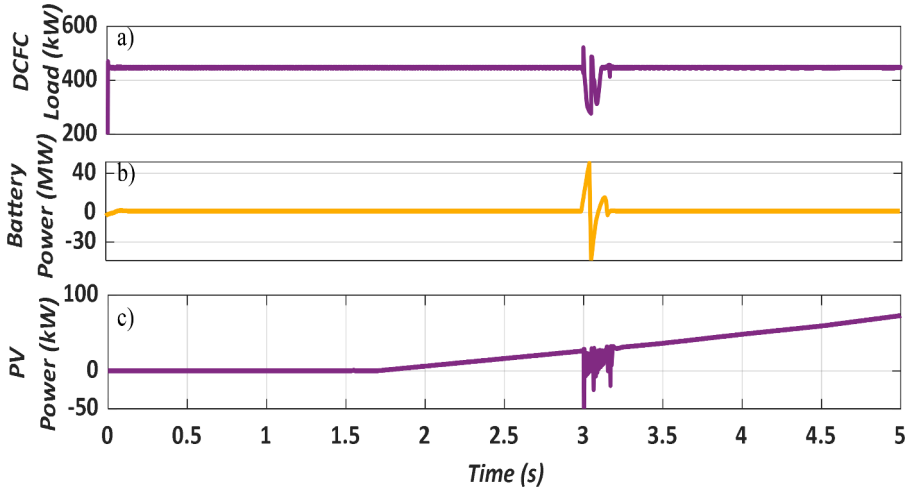

Fig. 11. Results for Case 1c a) DCFC load b) P battery c) P from solar PV system.

established between positive and negative poles as the conductors come in direct contact with each other somehow. PG faults are known as High Impedance Faults (HIF) because the connection of one or both conductors is established with the ground, for instance, the conductors fall to the ground or a human body, tree, or a bird come in contact with poles. The impedance of the DC microgrid is low; therefore, a large surge in fault current takes place because of the fast discharging of capacitive filters linked to the converters [1,2]. As a result, converters can get damaged due to sustained faulty conditions and the system may enter an unstable mode of operation. In DC microgrid systems, the magnitude and severity of fault current is higher in case of occurrence of low impedance fault i.e., PP faults.

The magnitude of fault current in DC microgrid system depends on control schemes, converters' topology, grounding type, impedance, location and type of fault, capacitors used in the system, DC bus voltage magnitude, and renewable energy source type [5]. The factors affecting fault current magnitude during line/pole to ground fault are the topology of the system, grounding, and voltage of DC bus. As indicated by

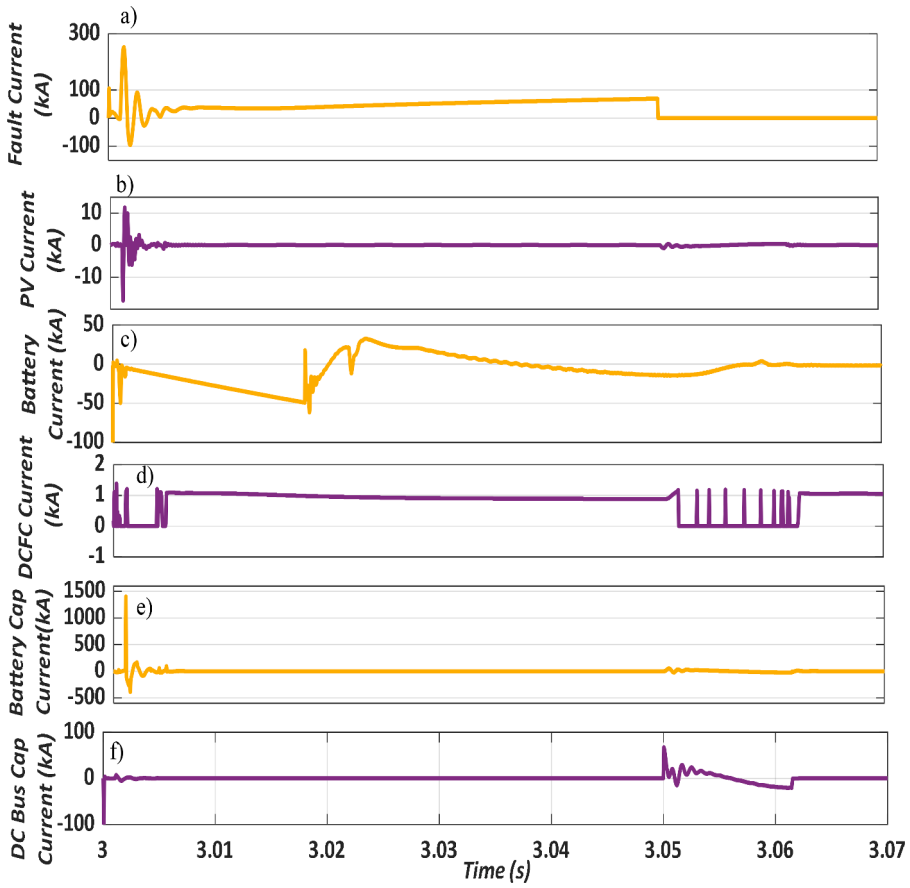

Fig. 12. Results for Case 1c. a) Fault current b) Current through PV system c) Current through battery system d) Currents through DCFC e) current through capacitor at battery terminals f) current through capacitor at DC link.

previous researchers, the value of fault current tolerated by typical VSC (Voltage source converters) is double the full load current rating of converters and the fault should be cleared in approximately 2 ms [6].

According to [6], PG faults occur more frequently in industrial systems. The impedance of pole-to-ground faults may be low. Whereas, the location of the fault can be a feeder, bus, or inside the converters [7]. Since there is very limited tolerance of over current by the electronic equipment, the gravity of the situation increases if the fault is located near the source of energy, in this way, the most critical fault location for the whole microgrid system can be considered at the DC bus as it has a direct impact on all the equipment connected to it [6,7]. However, if there is a fault in the feeder, the continuation of supply to healthy feeders can be disrupted. The occurrence of terminal faults such as faults inside the batteries and converters may result in PP faults. There may be a need for the replacement of equipment after terminal faults as the clearance of those faults is not fast enough. Fuse deployment may be an appropriate solution for the protection of equipment in such cases. In DC microgrids, the PP fault is the most classical one. The response to this type of fault can be categorized into three stages, discharging of capacitors, freewheeling of diodes, and current feeding from the grid side.

PP Faults have been simulated at various locations in this study. The fault locations F_1, F_2, F_3, and F_4 are (depicted in Fig. 2) correspond to solar PV, DC bus, EV load, and battery system respectively. Similarly, the simulation locations for PG faults are shown in Fig. 3. Resistance pertaining to skin contact has a value ranging from 1000 Ω to 100,000 Ω, subject to various factors, including skin conditions, moisture, and contact area [7]. However, a resistance of 1000Ω is modeled to account for high impedance during PG faults. During steady-state conditions, DC cables are generally resistive. However, to take into consideration transient behavior of cable during a fault, it has been represented as its pi-model comprising resistance, capacitor, and inductor using parameters available in the literature [9,10]. In the DC system under study, the distance between the DC bus and solar PV and EV load canopy is 40 m and the distance of BESS from the DC bus is 20 m. The resistance and inductance of cables are 0.641Ω/km and 0.34mH/km respectively [8]. Further, we have carried out these simulations for fault durations of 10 ms and 50 ms to assess the behavior and ability of controllers to bring the system back to the region of stability in the event of a fault and the minimum requirements of fault clearing time for DC breakers to be installed for system protection.

For all scenarios, the cases have been simulated in such a way that, at the start of simulation from 0 to 3 s, the system is operating under normal conditions. The battery system is regulating the DC bus voltage while the converter is receiving P and Q set points). EV load is kept constant and variations in the output of solar PV are taking place. At the 3rd s, a fault is introduced at one of the locations by connecting its positive terminal with the negative one. After 10 ms or 50 ms, the fault is cleared. Total simulation time is kept as 5 s. For analysis purposes, the results have been presented in three figures for each case. One of the figures presents active (P), reactive power (Q), Voltage (V_{ac}), and Current (I_{ac}) on the AC side, DC bus voltage, DC bus current, and Total Harmonic Distortion (THD). The positive sign of P and Q represents the flow of P and Q from DC to AC side and negative sign indicates the reverse flow i.e., flow of P and Q from AC to DC side. DC Fast Charger (DCFC) or EV load, power from the battery, and solar PV are shown in the second figure. In the third one, fault currents measured at various locations have been plotted. For instance, the first subplot presents the fault current at the fault location (point of fault). In the second subplot, the current at the output terminals of the PV system has been shown, the third subplot corresponds to the current measured at the output

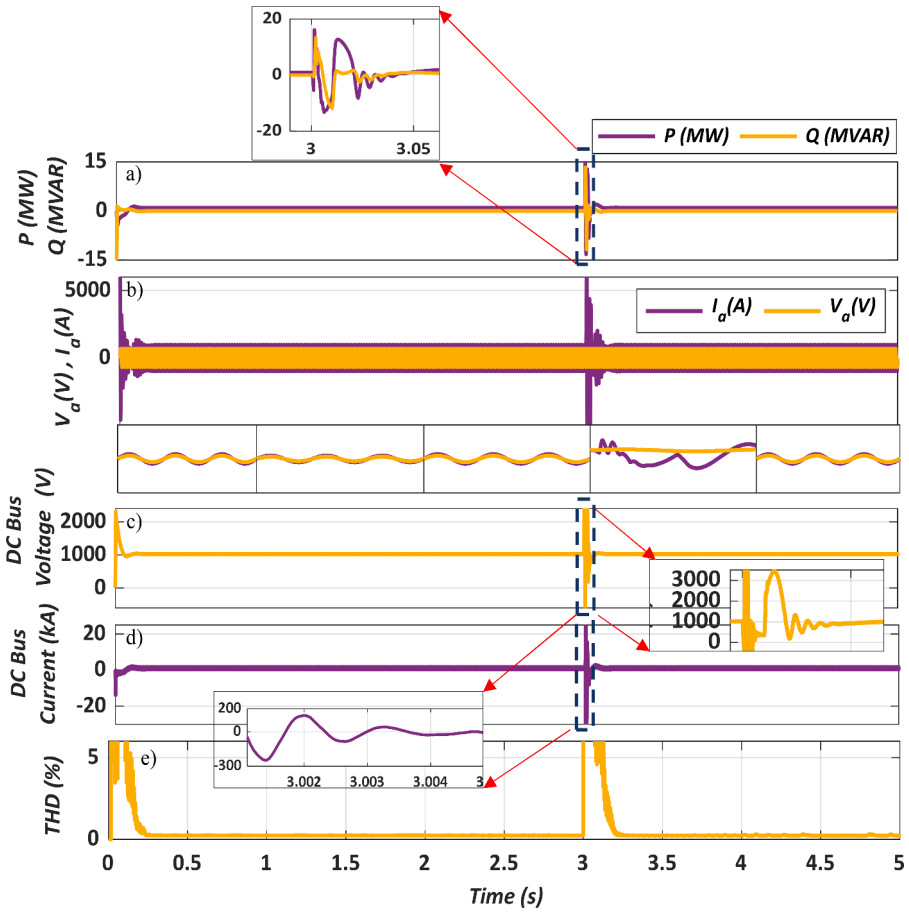

Fig. 13. Results for Case 1d a) P, Q b) V_{ac}, I_{ac}, c) DC bus voltage d) DC bus current e) THD.

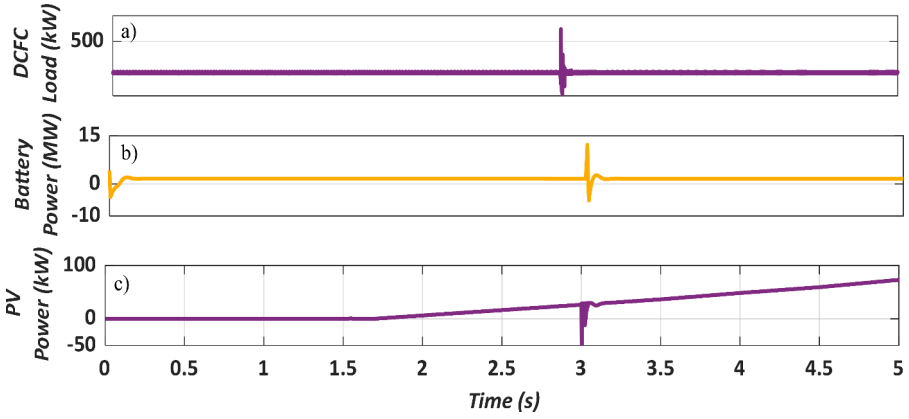

Fig. 14. Results for Case 1d a) DCFC load b) P battery c) P from solar PV system.

terminals of the battery system. In the fourth subplot, the current of the EV load measured at the point before the DC-DC converter can be seen. Since, discharging of DC capacitors can increase fault current significantly; therefore, currents through DC capacitors connected across the DC bus and at the output of the battery system need to be analyzed. These have been plotted in subplots five and six, respectively.

Case 1: Low Impedance (PP) Faults

a) *Fault Location: DC bus, Fault Duration:* 10 ms

The fault location is the DC bus. Fig. 4 shows *P* and *Q*, V_{ac}, I_{ac}, DC bus voltage, current through DC bus and% THD. It is evident from this figure that there is a spike in all measurements at 3 s. However, after fault clearance, they become stable as in pre-fault conditions. Similarly, a spike in EV load, power from the battery, and solar PV output power can also be observed in Fig. 5. To have a detailed fault analysis, current through DC bus, current from solar PV, EV load, battery system, capacitors at battery system and DC bus have been plotted in Fig. 6. It can be observed in Fig. 6 that fault current through DC bus reaches slightly above than 1000 kA at approximately. 3.004 s (in 4 ms). Whereas maximum values achieved by current flowing through solar PV system is approximately. 8kA at 3.01 s. Even though PV current is limited by short circuit capacity of PV. The current in the figure presents current in the whole PV system and spike is attributed to the discharge current of the

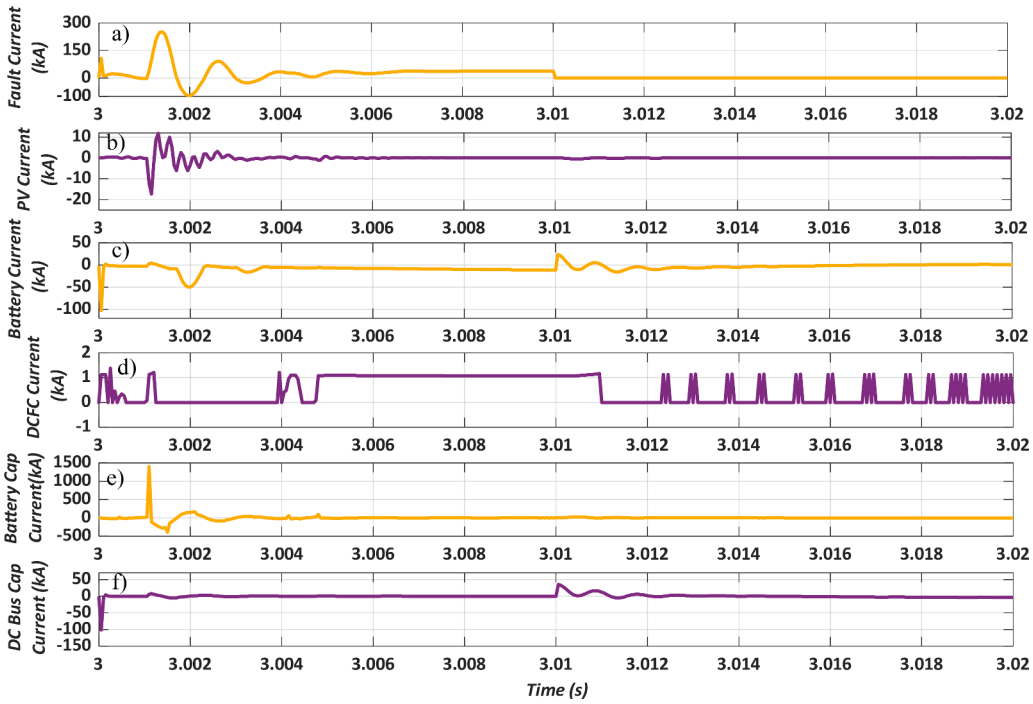

Fig. 15. Results for Case 1*d* a) Fault current b) Current through PV system c) Current through battery system d) Currents through DCFC e) Current through capacitor at battery terminals f) Current through capacitor at DC link.

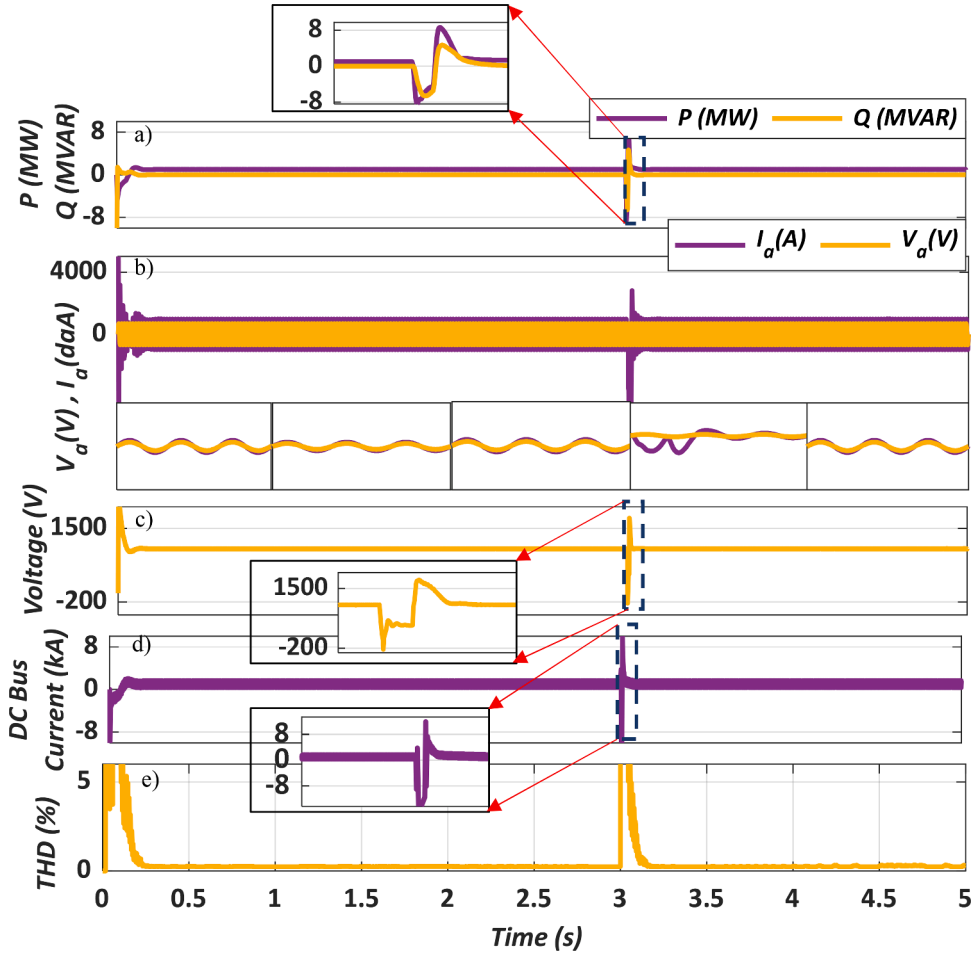

Fig. 16. Case 1*e. a) P, Q* b) V_{ac}, I_{ac}, c) DC bus voltage d) DC bus current *e)*%THD.

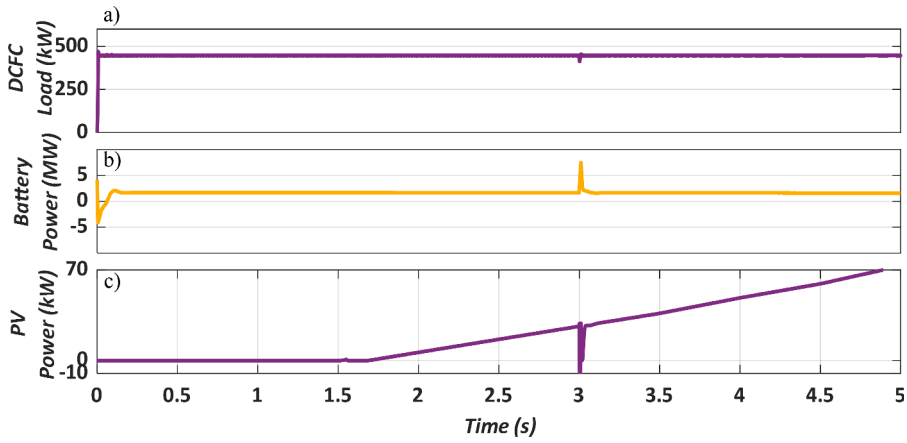

Fig. 17. Results for Case 1e. a) DCFC load b) P battery c) P from solar PV system.

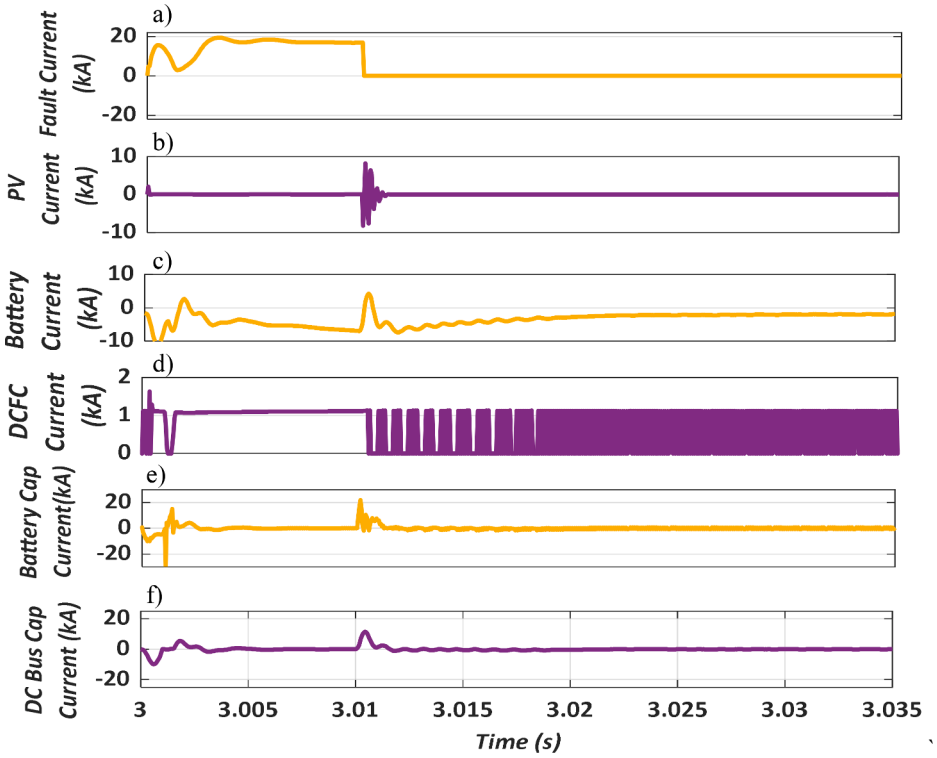

Fig. 18. Results for Case 1*e*. a) Fault current b) Current through PV system c) Current through battery system d) Currents through DCFC e) Current through capacitor at battery terminals f) Current through capacitor at DC link.

capacitor. During fault, maximum current in the battery system is around 80kA. The magnitudes of currents discharged by the capacitor connected to the battery system and DC bus can also be observed in the same figure which are of the order of 1100kA and 80kA respectively. During the fault, P flow is negative which shows that it flows from AC side to DC side to feed the fault. It can be seen from the figure that the power coming from AC side not only feeds the fault but also charges the capacitor at the output terminals of the battery. After 3.01 s, current flows out of the battery terminals which charges the DC bus capacitor. A relatively small amount of current also comes out of the PV system terminals. During the fault, the AC-DC converters needs to be isolated to avoid large surge of current.

a) *Fault Location: DC bus, Fault Duration:* 50 ms

Fig. 7 shows that there are spikes in P and Q, V_{ac}, I_{ac}, DC bus voltage, current through DC bus and% THD at 3 second. However, stable results are achieved again after fault clearance. Similarly, from Fig. 8a spike in EV load, power from battery and solar PV output power can also be observed. The values of instantaneous in/out flows of power from the battery system are of the order of 39MW at 3 s. Fig. 9 shows current through DC bus, solar PV, EV load and battery system. It is evident from the figures that fault current through DC bus attains the maximum value 2500kA 3.006 (in 6 ms) which is in reverse direction. The fault current flowing from negative pole towards the positive pole. The capacitor coupled with DC bus is also discharged. Real power (P) flows towards the AC side from DC side which can be seen in Fig. 7 (subplot 1). During the fault at DC bus, current through solar PV is very small of the order of 1–2kA only. Whereas maximum value achieved by the current going into battery system after the fault is approximately 20kA at 3.006 s. It can be seen from the figure that the during fault, DC bus current is negative and power coming from AC side not only feeds. The huge

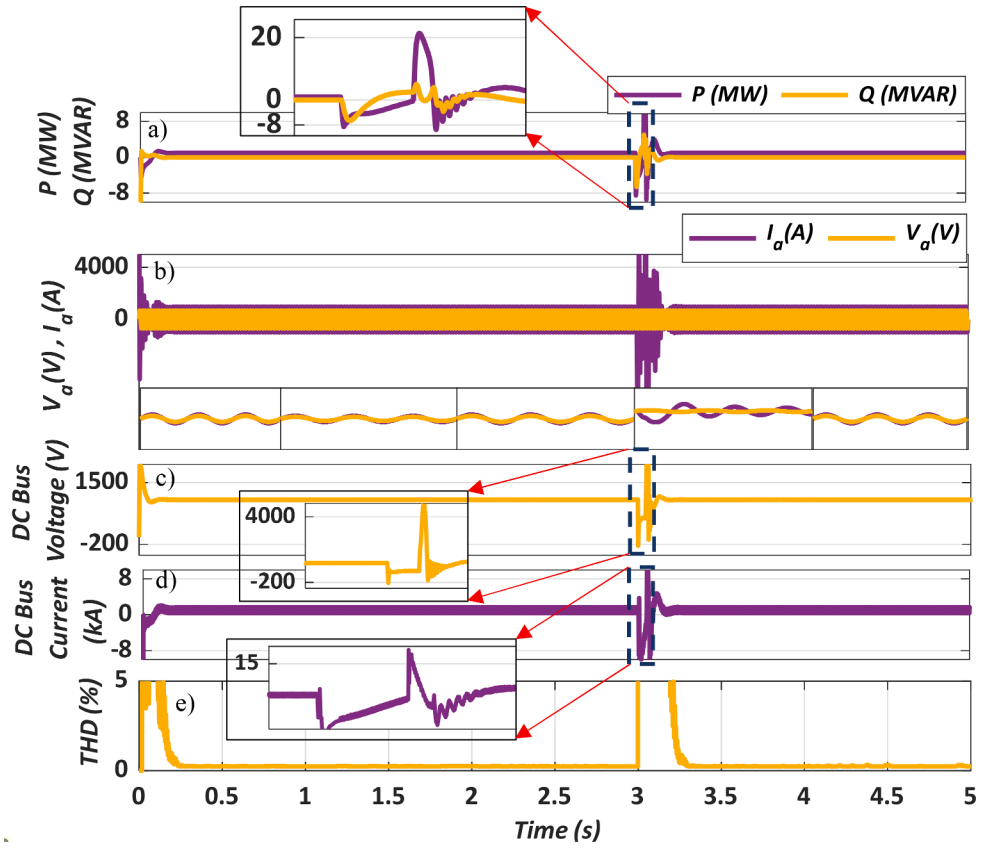

Fig. 19. Results for Case 1f (a) P, Q b) V_{ac}, I_{ac}, c) DC bus voltage d) DC bus current e)%THD.

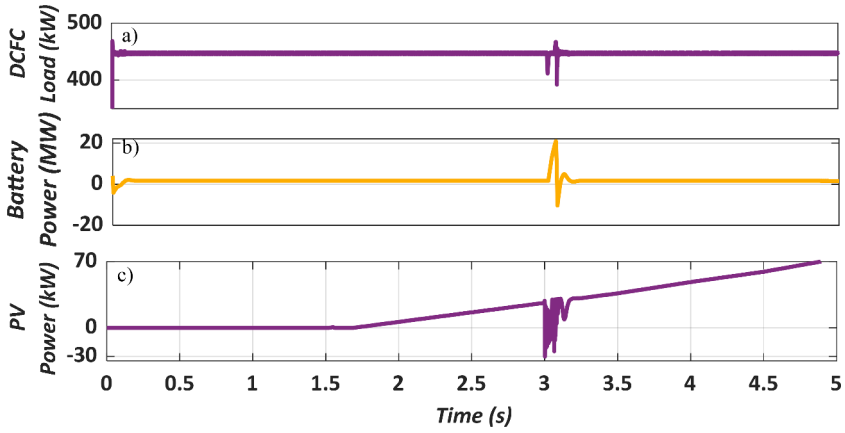

Fig. 20. Results for Case 1f. a) DCFC load b) P battery c) P from solar PV system.

amount of discharging current also flows from the capacitors connected to the battery and DC bus. During the fault, the AC-DC converters needs to be isolated to avoid the flow of large surge of current from one side to another.

a) *Fault Location: BESS, Fault Duration:* 50 ms

The fault location is output terminals of battery system and duration is 50 ms. Disturbance can be observed in *P* and *Q*, V_{ac},I_{ac}, DC bus voltage, current through DC bus and% THD at 3 s in Fig. 10. However, after fault clearance, they are settled again. Similarly, Fig. 11 shows the impact of fault on EV load, power from battery and solar PV output power. Approximately 40MW of instantaneous power flows in and out of from the battery system at 3 s. Fig. 12 shows the fault current, current through solar PV, battery system, and EV system. It can be observed that fault current through the battery system keeps on increasing gradually and reaches the maximum value of around 80 ms in 3.05 s (50 ms). During these 50 s, the current is continuously increasing until the fault is interrupted at 3.05 s. Hence, it is suggested that the fault current must be interrupted quickly to avoid the large magnitudes hence damage. The fault current flows into the battery terminals. After that, there is an outflow of current is observed from the battery after 3.05 s. After 3.05 s, the DC bus capacitor and capacitor connected to the battery are discharged. The current discharged by the capacitor connected with battery (subplot 5) goes out of the terminals of the battery (subplot 3) and flows towards the AC side. This can be seen in Fig 10 sublot 1. There is a surge of power (bump) in the graph after 3.05 s tilt 3.065 s. After that the P and Q flows come back to the pre-fault value. During the fault, there is a

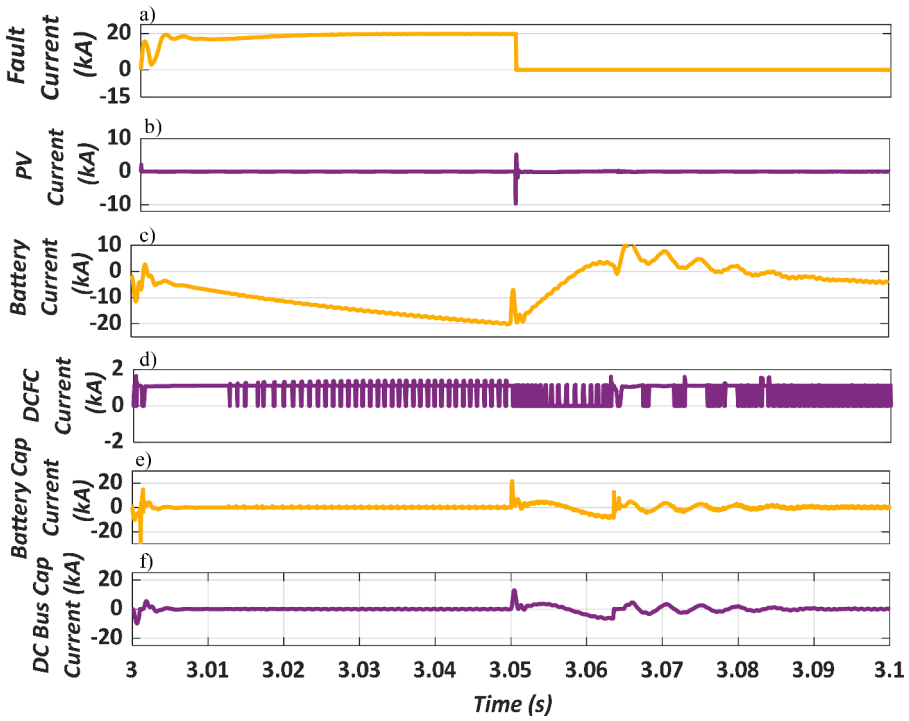

Fig. 21. Results for Case 1*f*. a) Fault current b) Current through PV system c) Current through battery system d) Currents through DCFC e) Current through capacitor at battery terminals f) Current through capacitor at DC link.

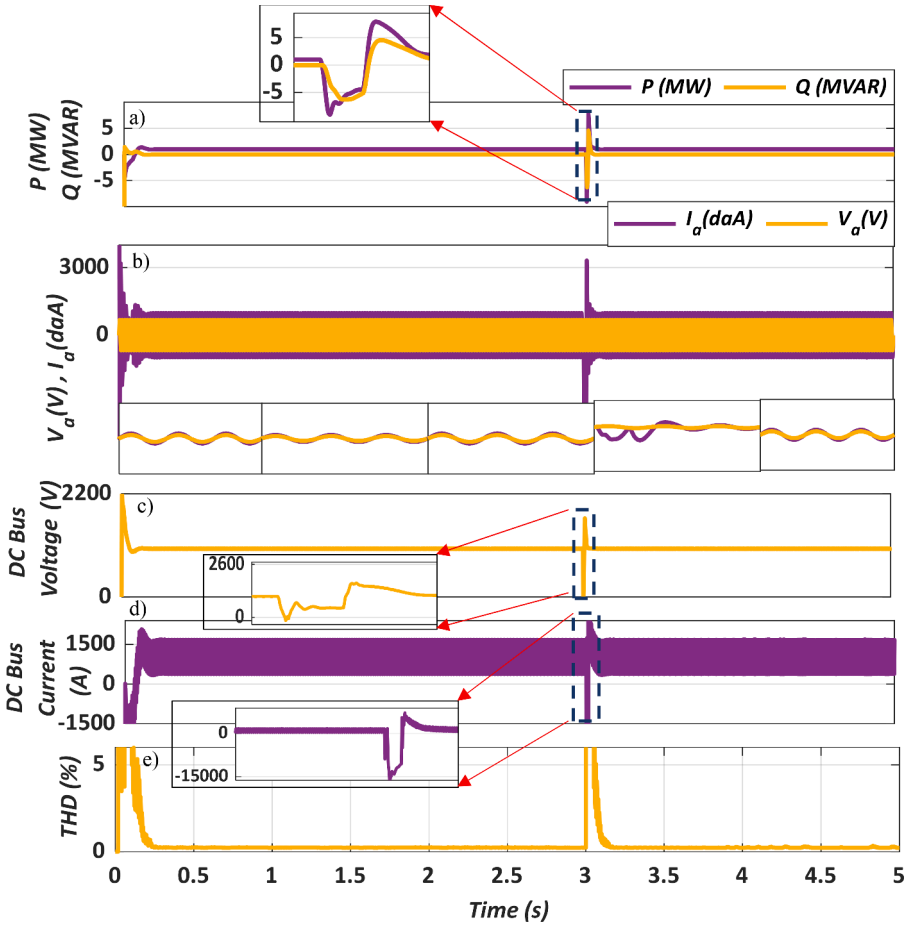

Fig. 22. Results for Case 1 g a) P, Q b) V_{ac}, I_{ac}, c) DC bus voltage d) DC bus current e)%THD.

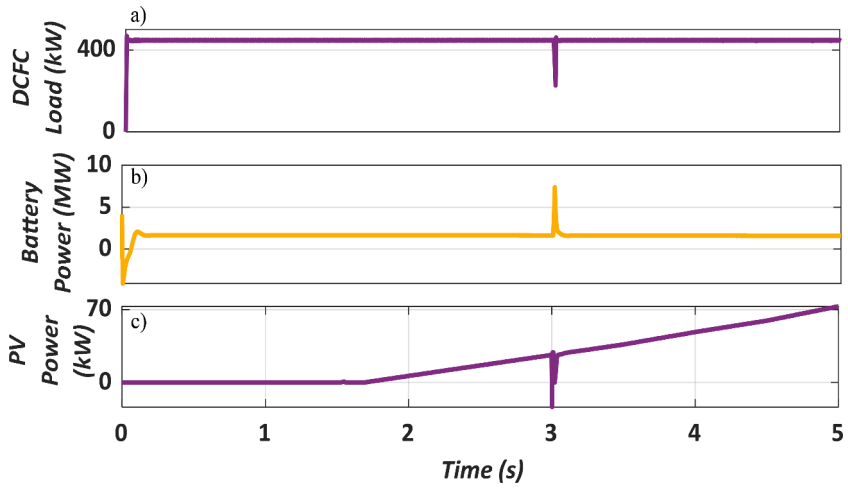

Fig. 23. Results for Case 1 g (a) DCFC load b) P battery c) P from solar PV system.

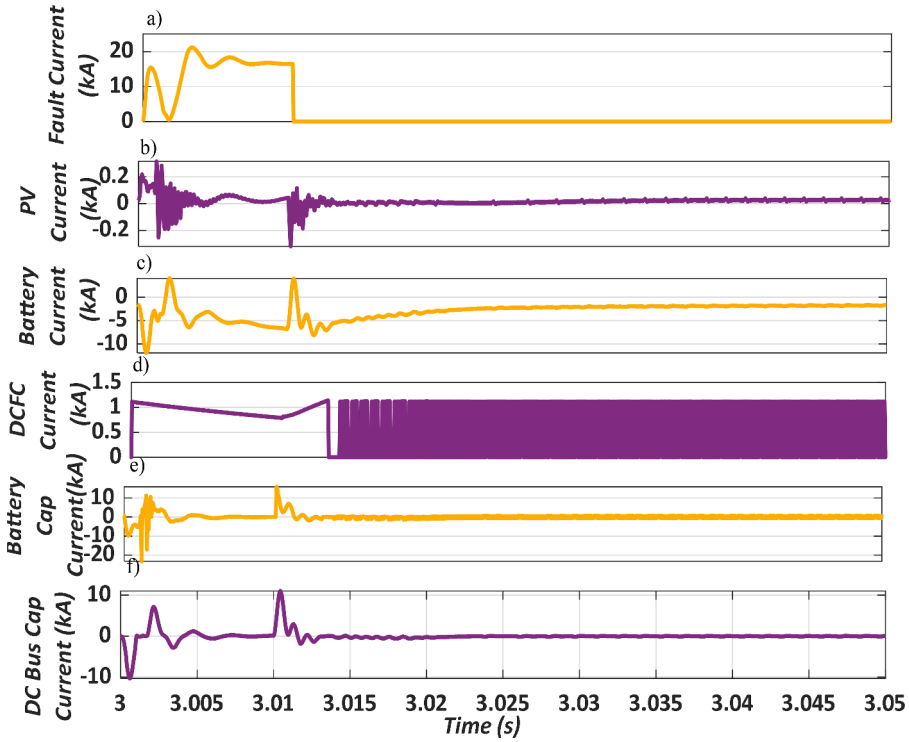

Fig. 24. Results for Case 1 g. a) Fault current b) Current through PV system c) Current through battery system d) Currents through DCFC e) Current through capacitor at battery terminals f) Current through capacitor at DC link.

surge in the value of DC bus voltage, it is due to large amount of injection of reactive and real powers. Maximum values of currents discharged by the capacitor connected to the battery system and DC bus voltage can also be observed.

a) *Fault Location: BESS, Fault Duration:* 10 ms

The impact of fault at the 3 s on *P* and *Q*, V_{ac}, and I_{ac}, DC bus voltage, the current through DC bus, and THD are depicted in Fig. 13. After fault clearance, their values return to their original values. Similarly, Fig. 14 shows the impact of fault on EV load, power from the battery, and solar PV output power. The values of instantaneous in/outflows of power from the battery system are of the order of 18MW at 3 s. During the occurrence of the fault, the current through the battery system, output terminals of solar PV, EV load, and battery system have been plotted in Fig. 15. Fault current through the battery system (reaches the maximum value of almost 30kA at approximately 3.004 s (in 4 ms), which is a very small duration. During the fault Fig. 13 (first subplot) shows that, during fault, current flows from AC to DC side, this flow of power feeding the fault current. At 3.01se, fault current becomes zero, current flows out of the battery Fig. 15 (3rd subplot), which goes to the DC bus capacitor for its charging. The current also flows to the capacitor connected to the battery for a moment.

a) *Fault Location: Solar PV System, Fault Duration:* 10 ms

The fault location is the output terminals of the PV system. Fig. 16 shows that a spike can be observed in *P, Q,* V_{ac}, I_{ac}, DC bus voltage, the current through the DC bus, and THD at the 3 second. However, after fault clearance, they settle again. Similarly, from Fig. 17, a spike in EV

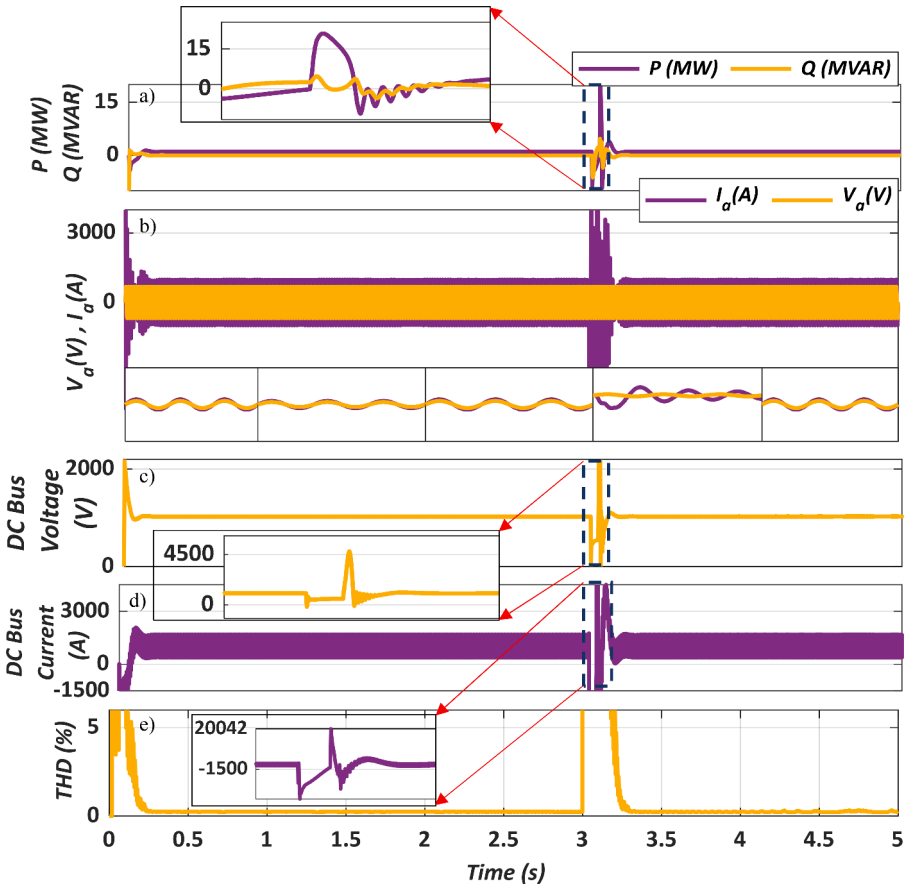

Fig. 25. Results for Case 1 h (a) P, Q b) V_{ac}, I_{ac}, c) DC bus voltage d) DC bus current e)%THD.

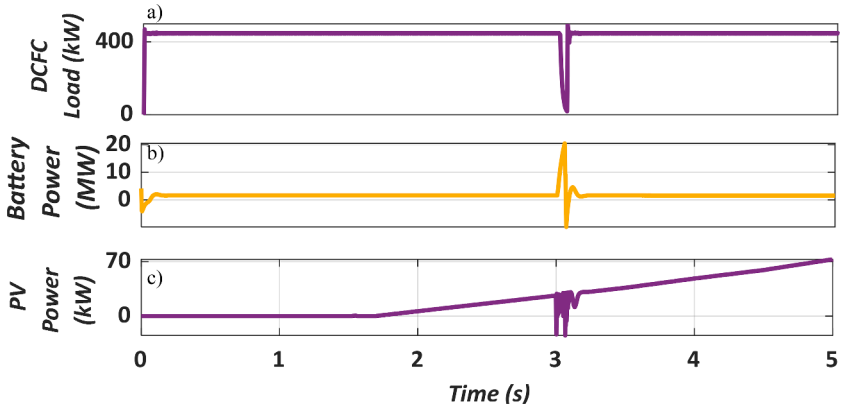

Fig. 26. Results for Case1*h* a) DCFC load b) *P* battery c) *P* from solar PV system.

load, power from the battery, and distortion in solar PV output power can also be observed. The values of instantaneous in/outflows of power from the battery system are of the order of 8MW at 3 s. In order to analyze the fault currents, currents through solar PV system, current EV load, and battery system have been plotted in Fig. 18. It can be observed that the fault current through the PV system reaches the maximum value (around 20kA) in approximately 4 ms (at. 3.004 s). The maximum values of currents discharged by the capacitor connected to both the battery system and DC bus are around 28kA and 14 kA respectively. During the fault, Fig. 16 (subplot 1), *P* flows from AC side to DC side till 3.01 s, after that, direction of flow reverses, it flows from DC to AC side. After clearance of fault 3.01 s, a transient is observed in capacitors connected to DC bus and battery. A surge in the current is observed which is going into the battery is observed. Some of this current is flowing towards DC bus capacitor.

a) *Fault Location: PV System, Fault Duration:* 50 ms

Results of this scenario are presented in Fig. 19 where *P* and *Q*, V_{ac}, I_{ac}, DC bus voltage, current through DC bus, and% THD goes through a disturbance at the 3rd second. After fault clearance, they become stable again. Similarly, the impact of fault on EV load, power from a battery and solar PV output power can also be observed in Fig. 20. The values of instantaneous in/outflows of power from the battery system are of the order of 20MW at 3 s. To analyze the fault current i.e., current through the point of fault, current during fault through solar PV system, current

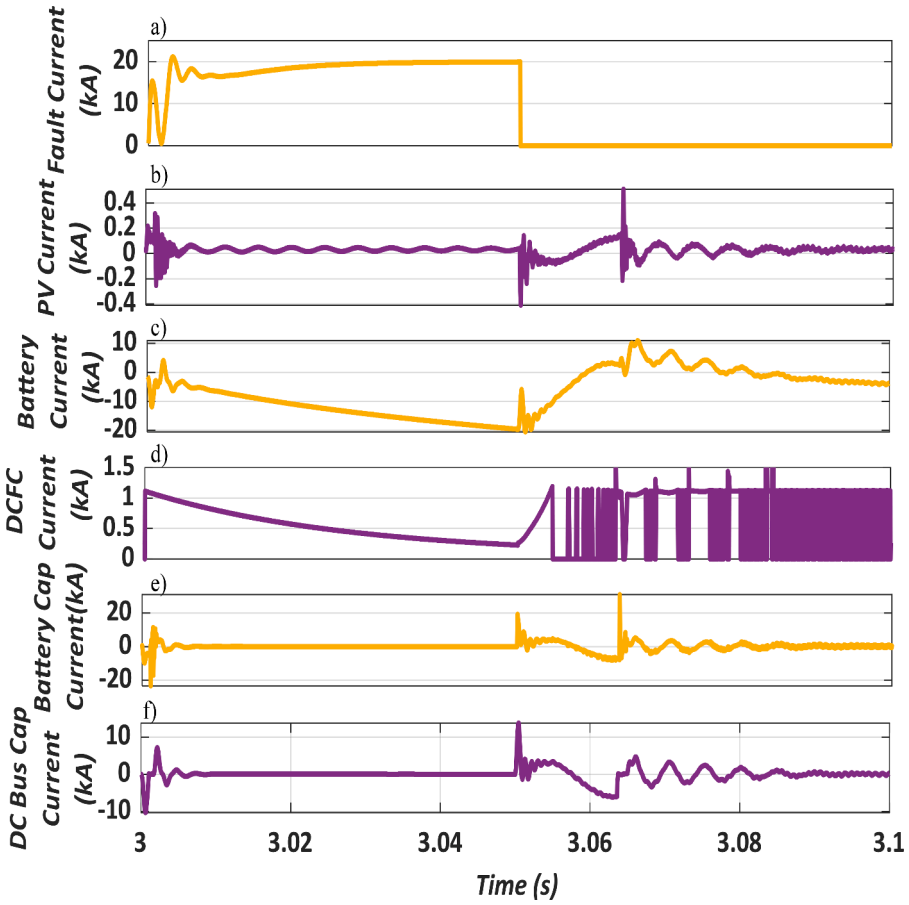

Fig. 27. Results for Case 1 h. a) Fault current b) Current through PV system c) Current through battery system d) Currents through DCFC e) Current through capacitor at battery terminals f) Current through capacitor at DC link.

at EV load and battery system, capacitors have been plotted in Fig. 21. It can be observed that fault current reaches the maximum value of around 20kA at approximately. 3.0025 s (2.5 ms). In Fig. 19 (subplot 1) shows that from 3 s to 3.05 s, power will flow from AC side to DC side and flows into the battery. Then there is a spike in value of *P* and it flows from DC to AC side (positive value). During these times, relatively small amount of current is also going towards the capacitors.

a) *Fault Location: EV System Fault Duration:* 10 ms

The fault location is the EV system's output terminals. Fig. 22 shows that when the fault is applied to the system at 3 s, a spike can be observed in *P, Q,* V_{ac}, I_{ac}, DC bus voltage, the current through the DC bus, and THD. However, after fault clearance, these stabilize again. Similarly, from Fig. 23, a spike in EV load, power from the battery, and distortion in solar PV output power can also be observed. The values of instantaneous in/outflows of power from the battery system are of the order of 7MW at 3 s. During the event of fault, fault current flowing through the EV system, current through solar PV, and current through output terminals of the battery system has been plotted in Fig. 24. Fault current through EV system decreases during the fault. After 3.01 s, the EV current increases and regain its original value. The currents for charging and discharging of both capacitors connected to the battery system and DC bus can be observed in Fig. 24.

a) *Fault Location: EV System Fault Duration:* 50 ms

The results corresponding to a fault duration of 50 ms are depicted in Fig. 25. At 3 s, a spike can be observed in *P, Q,* V_{ac}, I_{ac}, DC bus voltage, current through DC bus, and THD. However, after fault clearance, stability is achieved. Similarly, from Fig. 26, a spike in EV load, power from the battery, and distortion in solar PV output power can be observed. The values of instantaneous in/outflows of power from the battery system are of the order of 25MW at 3 s. During the fault, the current flowing through the EV system, the current through the solar PV, the current through the output terminals of the battery system, BESS, and DC bus capacitors have been plotted in Fig. 27. It is evident that the fault current through the EV system reaches values higher than 20kA at approximately 3.003 s (in 3 ms) as indicated by the negative peak in Fig. 27. The DCFC current decreases during fault and after 3.05 s, resumes its value. The currents discharged by both capacitors connected to the battery system and the DC bus can be observed in Fig. No 27.

Case 2. High Impedance Fault (HIF)

As discussed earlier, high impedance faults, (e.g., human body faults or tree touching) may be challenging to detect because of the low value of fault current, which can be easily mistaken with large load changes. HIFs have been simulated at various locations as depicted in Fig. 3. However, it is worth mentioning that no significant impact on the *P, Q,* V_{ac}, I_{ac}, DC bus voltage, current through DC bus, and THD was observed. Results pertaining to a sample of the locations of the faults are presented below to avoid redundancy, as the same response has been observed for each location. Here, simulation results of the fault applied at the DC bus have been presented and the fault lasts for 50 ms. Fig. 28 shows *P, Q,* V_{ac}, I_{ac}, DC bus voltage, the current through the DC bus, and THD. It is evident from Fig. 28. that there is no spike in any measurements at the 3 second as opposed to the results pertaining to LIF. Similarly, EV load, power from the battery, and solar PV output power can also be observed in Fig. 29. The current through the DC bus, the current from solar PV, EV load, battery system, capacitors at battery system, and DC bus have been plotted in Fig. 30. It can be observed in Fig. 30 that fault current through

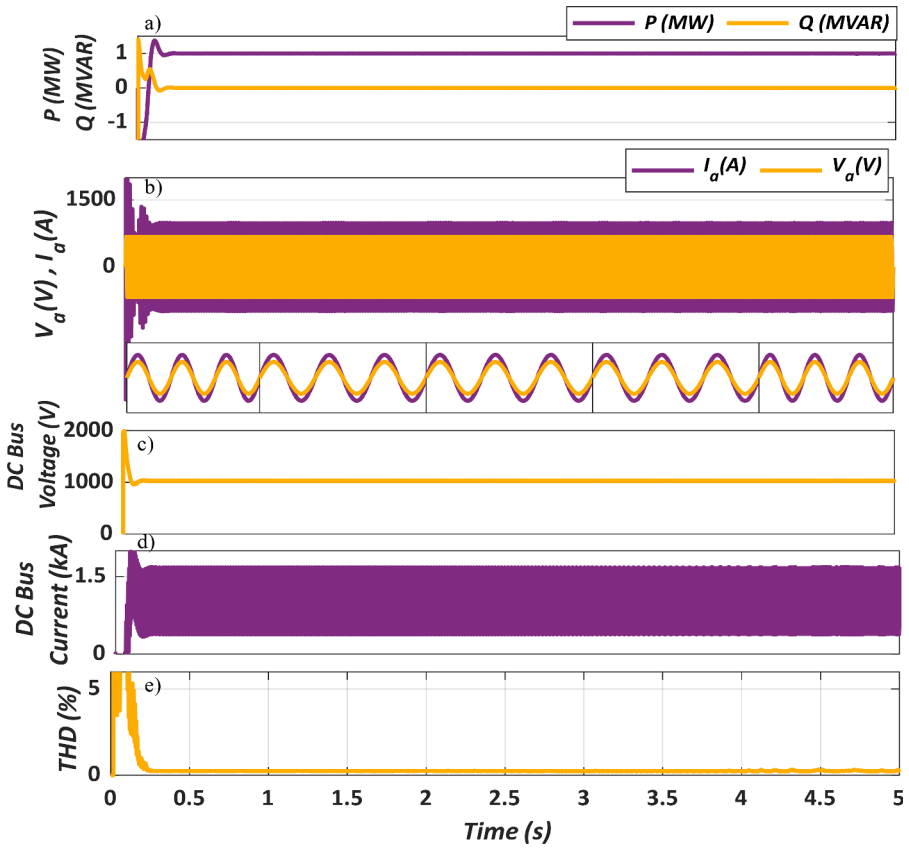

Fig. 28. Results for Case 2 a) P, Q b) V_{ac}, I_{ac}, c) DC bus voltage d) DC bus current e)%THD.

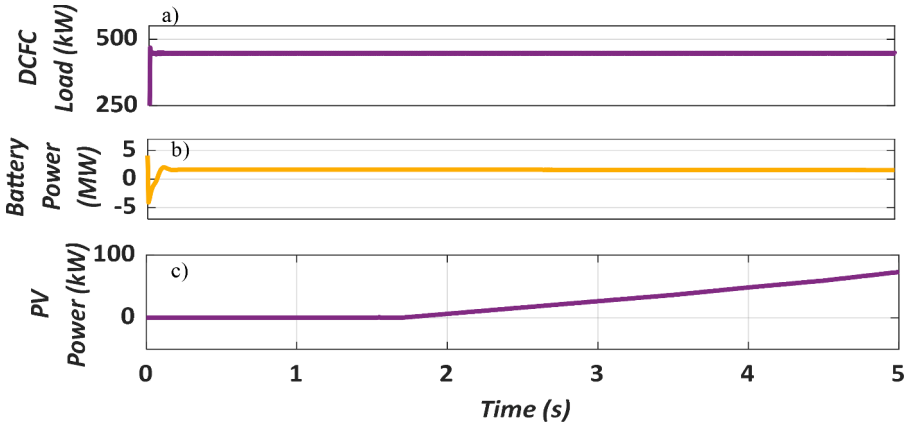

Fig. 29. Results for Case 2. a) DCFC load b) P battery c) P from solar PV system.

DC bus is just 1A.

The results of fault analysis are summarized in Table II. As shown, most severe fault is the fault at the DC bus. The time duration also plays a role in making the case worst, i.e., the longer it takes to clear the fault, the higher the value it achieves. Therefore, very fast acting protection equipment is required to ensure stability of the system and avoid the damage to the system due to high flows of currents. The fault current levels at PV and EV systems are nearly equal. The duration of fault does not affect the severity. It is difficult to detect the HIF because its value is quite low.

5. Conclusion

In this study, two types of faults have been simulated with two different time durations at various locations of DC bus system. It is evident from the results that when fault duration is more, higher values of currents in the system can be observed during faults. Further, for low impedance faults, the rate of rise of fault current is very high (few ms) and large peaks can be observed. Therefore, solid-state DC breakers with ultra-high speed must be deployed for prompt detection/isolation of faults. On the other hand, the value of fault current in the case of high impedance fault is very low, which makes its identification quite challenging. The topology and configuration of DC bus systems, converters, type of sources connected with DC bus, control, and grounding schemes are some of the factors affecting fault current levels. Although the studies have been carried out considering actual system to be installed at one of the substations of Con-Edison. And the equivalent model of substation has been modeled using R/X ratio of the substation. However,

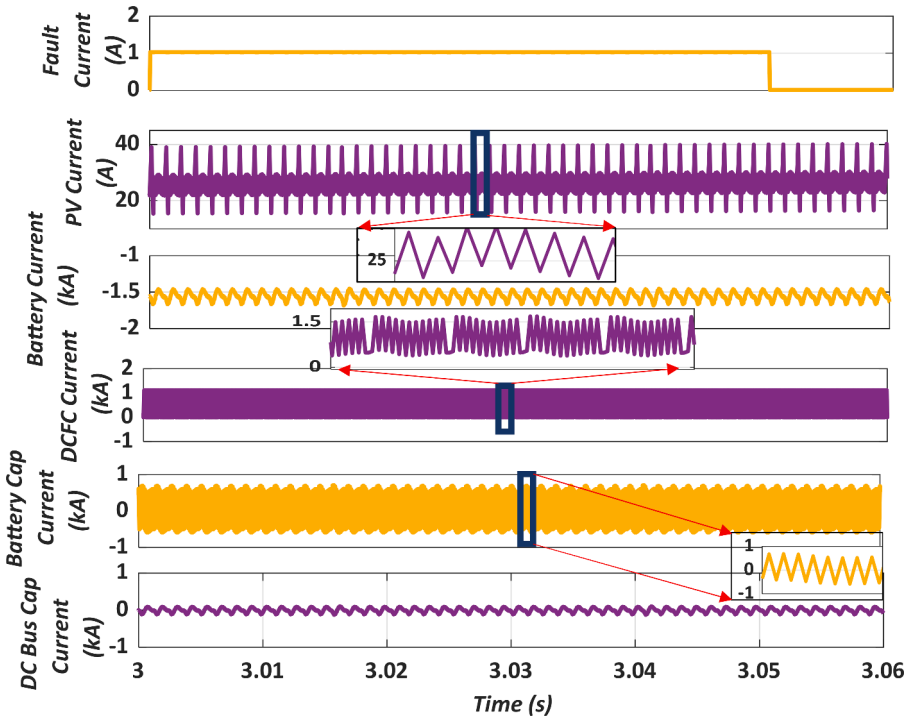

Fig. 30. Results for Case 2. a) Fault current b) Current through PV system c) Current through battery system d) Currents through DCFC e) Current through capacitor at battery terminals f) Current through capacitor at DC link.

Table II
Maximum Fault Current Values.

Sr. No	Fault Type	Fault Location	Duration of Fault	Maximum Value
1	Low Impedance Fault	DC Bus	10 ms	1000 kA
2		DC Bus	50 ms	2500 kA
3		BESS	50ms	79 kA
4		BESS	10 ms	30 kA
5		solar PV	10 ms	20 kA
6		solar PV	50 ms	20 kA
7		EVCS	10ms	21 kA
8		EVCS	50 ms	21 kA
9	High Impedance Fault	DC Bus	50 ms	1A

more accurate modelling and simulations are required before procurement and installation of the protection equipment. For instance, actual specification of converters, DC link capacitors and grounding arrangements must be considered. Finally, protection schemes and protection equipment may be designed and deployed after comprehensive analysis. Once the system is installed, the real time data will be gathered to perform the comparison studies. The data may also be utilized to develop the digital twins. Further, the data driven, and physics informed machine learning based protection schemes may be investigated as future work.

CRediT authorship contribution statement

Kirn Zafar: Writing – original draft, Visualization, Validation, Software, Methodology, Investigation, Formal analysis. **Mohamed K. Kamaludeen:** Writing – review & editing, Supervision, Resources, Project administration, Formal analysis, Data curation, Conceptualization. **Yusef Esa:** Validation, Software, Resources, Methodology, Investigation, Formal analysis. **Ahmed Ali A. Mohamed:** Writing – review & editing, Supervision, Project administration, Investigation, Funding acquisition, Formal analysis, Data curation, Conceptualization. **Simon Odie:** Supervision, Resources, Project administration, Funding acquisition.

Declaration of competing interest

The authors declare no conflict of interest.

Data availability

The data that has been used is confidential.

References

[1] S. Beheshtaein, R. Cuzner, M. Savaghebi, J.M. Guerrero, Review on microgrids protection, IET Gen., Trans. Distri. 13 (6) (2019) 743–759.
[2] V. Nasirian, S. Moayedi, A. Davoudi, F. Lewis, Distributed cooperative control of DC microgrids, IEEE Trans. Power Electron. 30 (4) (Apr. 2015) 2288–2303.
[3] S. Beheshtaein, R.M. Cuzner, M. Forouzesh, M. Savaghebi, J.M. Guerrero, DC microgrid protection: a comprehensive review, IEEE J. Eme. Sele. Top. Power Elect. (2019), 1–1.
[4] M. Saleh, Y. Esa, A. Mohamed, Communication Based Control for DC Microgrids, IEEE Trans. Smart Grids 10 (2) (Jan. 2018) 2180–2195.
[5] L. Zhang, N. Tai, W. Huang, J. Liu, Y. Wang, A review on protection of DC microgrids, J. Modern Power Syst. Clean Energy 6 (6) (2018) 1113–1127.
[6] A. Chandra, G.K. Singh, V. Pant, Protection Techniques for DC microgrid-A Review, 187, Electric Power Systems Research, 2020 106439.
[7] R.M. Fish, L.A. Geddes, Conduction of electrical current to and through the human body: a review, Eplasty 9 (2009 Oct 12) e44. PMID: 19907637; PMCID: PMC2763825.
[8] S. Dhar, P.K. Dash, Differential current-based fault protection with adaptive threshold for multiple PV-based DC microgrid, IET Renew. Power Generat. 11 (6) (2017) 778–790.
[9] A.T. Elsayed, A.A. Mohamed, O.A. Mohammed, DC microgrids and distribution systems: an overview, Electr. Power Syst. Res. 119 (2015) 407–417.
[10] Chetan Srivastava, Manoj Tripathy, DC microgrid protection issues and schemes: a critical review, Renew. Sustain. Energy Rev. 151 (2021) 111546.
[11] Q.-C. Zhong, G. Weiss, Synchronverters: inverters that mimic synchronous generators, IEEE Trans. Ind. Electron. 58 (4) (April 2011) 1259–1267.
[12] K.E. Lucas-Marcillo, et al., Novel Robust Methodology for Controller Design Aiming to Ensure DC Microgrid Stability Under CPL Power Variation, IEEe Access. 7 (2019) 64206–64222.

[13] M. Dicorato, G. Forte, M. Trovato, C.B. Muñoz, G. Coppola, An integrated DC microgrid solution for electric vehicle fleet management, IEEE Trans. Ind. Appl. 55 (6) (Nov.-Dec. 2019) 7347–7355.
[14] D. Kumar, F. Zare, A. Ghosh, DC microgrid technology: system architectures, AC grid interfaces, grounding schemes, power quality, communication networks, applications, and standardizations aspects, IEEe Access. 5 (2017) 12230–12256.
[15] D. Salomonsson, L. Soder, A. Sannino, Protection of low-voltage DC microgrids, IEEE Trans. Power Deliv. 24 (3) (2009) 1045–1053.
[16] Z. Ali, Y. Terriche, S.Z. Abbas, M.A. Hassan, M. Sadiq, C.L. Su, J.M. Guerrero, Fault management in DC microgrids: a review of challenges, countermeasures, and future research trends, IEEe Access. 9 (2021) 128032–128054.
[17] E.W. Nahas, H.A. Abd el-Ghany, D.E.A. Mansour, M.M. Eissa, Extensive analysis of fault response and extracting fault features for DC microgrids, Alexandria Eng. J. 60 (2) (2021) 2405–2420.
[18] N. N Bayati, A. Hajizadeh, M Soltani, Fault analysis and protection of low-voltage DC microgrid equipped by renewable energy resources. Research Anthology on Smart Grid and Microgrid Development, IGI global, 2022, pp. 978–1012.
[19] N. Bayati, H.R. Baghaee, A. Hajizadeh, M. Soltani, Z. Lin, M. Savaghebi, Local fault location in meshed DC microgrids based on parameter estimation technique, IEEe Syst. J. 16 (1) (March 2022) 1606–1615, https://doi.org/10.1109/JSYST.2021.3107905.
[20] Younes Seyedi, Jean Mahseredjian, Houshang Karimi, Impact of fault impedance and duration on transient response of hybrid AC/DC microgrid, Electric Power Syst. Res. 197 (2021) 107298.
[21] N. Bayati, H.R. Baghaee, A. Hajizadeh, M. Soltani, Z. Lin, M. Savaghebi, Local fault location in meshed DC microgrids based on parameter estimation technique, IEEE Syst. J. 16 (1) (March 2022) 1606–1615, https://doi.org/10.1109/JSYST.2021.3107905.
[22] H. Han, et al., A fast fault diagnosis scheme for ring bus DC microgrids with fewer sensors, IEEE Trans. Power Deliv. 39 (1) (Feb. 2024) 283–295, https://doi.org/10.1109/TPWRD.2023.3333535.
[23] S.A. Wakode, M.S. Ballal, R.R. Deshmukh, Sliding DFT-based fault location scheme for DC microgrid, IEEE Trans. Ind. Appl. 58 (5) (2022) 5944–5954, https://doi.org/10.1109/TIA.2022.3189610. Sept.-Oct.
[24] S.K. Prince, S. Affijulla, G. Panda, Protection of DC microgrids based on complex power during faults in On/Off-Grid scenarios, IEEE Trans. Ind. Appl. 59 (1) (2023) 244–254, https://doi.org/10.1109/TIA.2022.3206171. Jan.-Feb.
[25] H.-C. Seo, Development of new protection scheme in DC microgrid using wavelet transform, Energies. (Basel) 15 (2022), https://doi.org/10.3390/en15010283.